Langmuir
Article
pubs.acs.org/Langmuir

Morphology and Stability of CO_2-in-Water Foams with Nonionic Hydrocarbon Surfactants

Stephanie S. Adkins,[†] Xi Chen,[†] Isabel Chan,[†] Enza Torino,[†] Quoc P. Nguyen,[‡] Aaron W. Sanders,[§] and Keith P. Johnston*,[†]

[†]*Department of Chemical Engineering, and* [‡]*Department of Petroleum and Geosystems Engineering, University of Texas, Austin, Texas 78712, and* [§]*The Dow Chemical Company, Freeport, Texas*

Received September 28, 2009. Revised Manuscript Received December 30, 2009

The morphologies, stabilities, and viscosities of high-pressure carbon dioxide-in-water (C/W) foams (emulsions) formed with branched nonionic hydrocarbon surfactants were investigated by in situ optical microscopy and capillary rheology. Over two dozen hydrocarbon surfactants were shown to stabilize C/W foams with Sauter mean bubble diameters as low as 1 to 2 μm. Coalescence of the C/W foam bubbles was rare for bubbles larger than about 0.5 μm over a 60 h time frame, and Ostwald ripening became very slow. By better blocking of the CO_2 and water phases with branched and double-tailed surfactants, the interfacial tension decreases, the surface pressure increases, and the C/W foams become very stable. For branched surfactants with propylene oxide middle groups, the stabilities were markedly lower for air/water foams and decane−water emulsions. The greater stability of the C/W foams to coalescence may be attributed to a smaller capillary pressure, lower drainage rates, and a sufficient surface pressure and thus limiting surface elasticity, plus small film sizes, to hinder spatial and surface density fluctuations that lead to coalescence. Unexpectedly, the foams were stable even when the surfactant favored the CO_2 phase over the water phase, in violation of Bancroft's rule. This unusual behavior is influenced by the low drainage rate, which makes Marangoni stabilization of less consequence and the strong tendency of emerging holes in the lamella to close as a result of surfactant tail flocculation in CO_2. The high distribution coefficient toward CO_2 versus water is of significant practical interest for mobility control in CO_2 sequestration and enhanced oil recovery by foam formation.

Introduction

Emulsions and foams of carbon dioxide and water, the two most plentiful solvents on earth, are of interest in a wide range of applications including CO_2 sequestration and enhanced oil recovery[1,2] green chemistry, materials science, microelectronics, and biotechnology.[3] CO_2 is an environmentally benign, essentially nontoxic, nonflammable, and recyclable solvent. The density of supercritical fluid carbon dioxide (T_c = 31 °C, P_c = 1070 psia (1 bar = 14.5 psia)) may be tuned over a wide range from gaslike to liquidlike values by varying the temperature and pressure.[4] Thus, the literature has referred to colloidal dispersions of water and carbon dioxide, at elevated pressures above 50 bar, as foams (to emphasize gaslike properties) or as emulsions (to emphasize liquidlike properties).[3] For simplicity, the term foam will be used most often in this study, whereas the term emulsion is just as appropriate. Carbon dioxide (CO_2) is miscible[5,6] in all proportions with the lighter hydrocarbon components of crude oil (up to 14 carbons depending on the system pressure) and partially miscible with heavier hydrocarbons,[7] which facilitates oil recovery from porous formations.[2]

The fundamental understanding needed for the design of surfactants for the stabilization of continuous aqueous films in carbon dioxide/water (C/W) foams/emulsions is still in its infancy.[2,8] An important distinction between C/W and air/water (A/W) foams is the marked difference in γ_o (without surfactant present) for the CO_2−water (C−W) (20 to 30 mN/m depending upon density) versus the air−water (A−W) interface (72 mN/m). The smaller γ_o for the C−W interface leads to a smaller driving force for surfactant adsorption to reduce the interfacial tension further.[9] Therefore, the area per surfactant molecule (A_m) at the C−W interface is often much larger than that at the A−W interface, as shown experimentally[10,11] and by molecular dynamics simulations.[12] Most studies of surfactants at the C−W interface have focused on W/C microemulsions.[13−22] In most

(1) Jarrell, P.; Fox, C.; Stein, M. *Practical Aspects of CO_2 Flooding*; Society of Petroleum Engineers; Richardson, TX, 2002; Vol. *22*.
(2) Rossen, W. R. Foams in Enhanced Oil Recovery. In *Foams: Theory, Measurements, and Applications*; Prudhomme, R. K., Khan, S. A., Eds.; Marcel Dekker: New York, 1996.
(3) Johnston, K. P.; Da Rocha, S. R. P. *J. Supercrit. Fluids* **2009**, *47*, 523–530.
(4) Eckert, C. A.; Knutson, B. L.; Debenedetti, P. G. *Nature* **1996**, *383*, 313–318.
(5) Yuan, H.; Johns, R. T.; Egwuenu, A. M.; Dindoruk, B. *SPE Reservoir Eval. Eng*. **2006**, *9*, 290.
(6) Yuan, H.; Johns, R. T.; Egwuenu, A. M.; Dindoruk, B. *SPE Reservoir Eval. Eng*. **2005**, *8*, 418–425.
(7) Heller, J. P. In *Foams: Fundamentals and Applications in the Petroleum Industry* ; Schramm, L. L., Ed.; Advances in Chemistry Series; American Chemical Society: Washington, DC, 1994; Vol. *242*, pp 201−234.
(8) Dhanuka, V. V.; Dickson, J. L.; Ryoo, W.; Johnston, K. P. *J. Colloid Interface Sci*. **2006**, *298*, 406–418.
(9) Rosen, M. J. *Surfactants and Interfacial Phenomena*, 3rd ed.; John Wiley & Sons: New York, 2004.
(10) Harrison, K. L.; Da Rocha, S. R. P.; Yates, M. Z.; Johnston, K. P.; Canelas, D.; DeSimone, J. M. *Langmuir* **1998**, *14*, 6855–6863.
(11) da Rocha, S. R. P.; Johnston, K. P. *Langmuir* **2000**, *16*, 3690–3695.
(12) da Rocha, S. R. P.; Johnston, K. P.; Rossky, P. J. *J. Phys. Chem. B* **2002**, *106*, 13250–13261.
(13) da Rocha, S. R. P.; Johnston, K. P. *Langmuir* **2000**, *16*, 3690–3695.
(14) da Rocha, S. R. P.; Harrison, K. L.; Johnston, K. P. *Langmuir* **1999**, *15*, 419–428.
(15) Stone, M. T.; da Rocha, S. R. P.; Rossky, P. J.; Johnston, K. P. *J. Phys. Chem. B* **2003**, *107*, 10185–10192.
(16) Dupont, A.; Eastoe, J.; Martin, L.; Steytler David, C.; Heenan Richard, K.; Guittard, F.; Taffin de Givenchy, E. *Langmuir* **2004**, *20*, 9960–9967.
(17) Sagisaka, M.; Fujii, T.; Ozaki, Y.; Yoda, S.; Takebayashi, Y.; Kondo, Y.; Yoshino, N.; Sakai, H.; Abe, M.; Otake, K. *Langmuir* **2004**, *20*, 2560–2566.
(18) Sagisaka, M.; Ozaki, Y.; Yoda, S.; Takebayashi, Y.; Otake, K.; Kondo, Y.; Yoshino, N.; Sakai, H.; Abe, M. *Mater. Technol. (Tokyo, Jpn.)* **2003**, *21*, 36–42.
(19) Dickson, J. L.; Smith, P. G., Jr.; Dhanuka, V. V.; Srinivasan, V.; Stone, M. T.; Rossky, P. J.; Behles, J. A.; Keiper, J. S.; Xu, B.; Johnson, C.; DeSimone, J. M.; Johnston, K. P. *Ind. Eng. Chem. Res*. **2005**, *44*, 1370–1380.

cases, fluorocarbon or siloxane surfactant tails were required to achieve sufficiently low γ values and reduce interdroplet interactions.[23−26] However, "stubby" hydrocarbon surfactants with branched and methylated tails block the interfacial contact of water and CO_2 more effectively than linear surfactants and thus may produce greater reductions in γ. Very low values of γ are required for W/C microemulsions with features smaller than 10 nm and high interfacial areas.[15,19,27,28] For C/W foams and emulsions with much lower specific surface areas, the amount of surfactant required to cover the interface is much smaller than for W/C or C/W microemulsions. Consequently, γ at the W−C interface may be much higher for C/W foams than for microemulsions. Thus, the requirements for surfactant design are much less stringent for foams than microemulsions. Furthermore, the formation of W/C microemulsions and macroemulsions is limited by the strong interdroplet tail−tail interactions, given the weak solvent strength of CO_2. For C/W foams and emulsions, the tails point inward into the CO_2 bubbles and these interactions have a much less severe influence on colloidal stability.

C/W emulsions (foams) with nonionic block copolymer stabilizers studied by da Rocha et al.[29] for up to 70% v/v CO_2 were stable against coalescence and flocculation for longer than 48 h. In addition, Dhanuka et al.[8] studied the hydrocarbon surfactant commercially known as Tergitol TMN 6 (Dow, 90% poly(ethylene glycol)-2,6,8-trimethyl-4-nonyl ether and 10% water w/w) as a stabilizer for 50−90% v/v CO_2 emulsions. Cell sizes of less than 10 μm were observed along with stability for longer than 24 h for a 90% v/v C/W foam.

The destabilization of foams (or concentrated emulsions) occurs via multiple mechanisms including drainage of the liquid in the lamella, coalescence of neighboring bubbles (lamella rupture), and Ostwald ripening. Coalescence may occur by spinodal decomposition when the attractive van der Waals forces between neighboring bubbles overcome the repulsive forces in the foam lamella.[30−33] With the appropriate stabilizers in the lamella, the foam can reach a metastable state.[34−36] Spatial and surface density fluctuations[37] may occur upon lamella drainage, leading to the formation of holes in the lamella,[32,38,39] and can induce spinodal decomposition.[31] The combined effects of thermodynamic and rheological properties on the stability of emulsions of oil and water are well known to be very complex and only partially understood.[31,35,40] These phenomena have received extremely little attention for emulsions/foams of water and CO_2. For C/W foams, we are not aware of any studies that have reported each of the key properties: foam texture (at the micrometer length scale), foam stability, interfacial properties, and foam viscosity.

The objectives of this study are to demonstrate that viscous C/W foams (emulsions) may be formed with over two dozen branched nonionic hydrocarbon surfactants and to evaluate various factors that influence foam stability, particularly, foam texture, phase behavior, and recent measurements of interfacial properties at the C−W interface.[41] These properties include γ, π, and the surfactant efficiency, pC20, which is the negative logarithm (base 10) of the molar surfactant concentration required to produce a 20 mN/m decrease in γ. Foams with greater than 90% v/v CO_2 were characterized by in situ optical microscopy over time periods from seconds to days for a cell path length of only 25 μm.[8] The viscosity, bubble size, and polydispersity are examined versus surfactant structure over a range of concentration, shear rate, temperature, salinity, and foam quality to characterize the aging mechanisms: drainage, coalescence, and Ostwald ripening. Stable foams are reported even for surfactants that favor the dispersed CO_2 phase over the continuous water phase.

For surfactants with branched tails, the stabilities of C/W foams are compared with those of much less stable A/W foams and O/W emulsions. The behavior is described in terms of the cloud-point temperature, surface pressure, Laplace pressure, and surfactant efficiency. As the distribution coefficient of the surfactant is shifted from hydrophilic to CO_2-philic with temperature, the C/W foam stabilities are shown to change very little in violation of Bancroft's rule. We attribute this unusual behavior to viscous stresses transmitted through each phase during emulsion formation, slow film drainage, and reduced hole formation and growth. The measurement and understanding of foam stability and viscosity are useful for the design of surfactants for CO_2 foam in enhanced oil recovery. In EOR, the surfactants in this study that are CO_2-soluble and favor CO_2 over water may be used to improve injectivity and mobility control in order to improve oil recovery.

Experimental Methods

Materials. Sodium chloride (GR, EM Science), calcium chloride dihydrate (certified A.C.S, Fisher), and magnesium chloride hexahydrate (enzyme grade, Fisher) were used as received. The surfactants (structures and naming schemes presented in Figure 1) were gifts from Dow and were used without any further purification. The subscripts denote the average number of repeat units per molecule based on the relative mass during synthesis. Research-grade carbon dioxide was passed through an oxygen trap (Oxyclear model RGP-31-300, Labclear, Oakland, CA) prior to use. Brine was made from deionized (DI) water (Nanopure II, Barnstead, Dubuque, IA) with 2% NaCl, 0.5% $CaCl_2$, and 0.1% $MgCl_2$ w/w in water (by weight). The symbol v/v means by volume in the aqueous phase for surfactants unless otherwise stated.

Cloud-Point Temperature. The cloud-point temperature of the aqueous surfactant solution was measured in a water bath equipped with a temperature controller. The surfactant concentration was 1.0% v/v in water for all samples. The error in the

(20) Psathas, P. A.; da Rocha, S. R. P.; Lee, C. T.; Johnston, K. P.; Lim, K. T.; Webber, S. E. *Ind. Eng. Chem. Res.* **2000**, *39*, 2655–2664.
(21) Psathas, P. A.; Sander, E. A.; Lee, M. Y.; Lim, K. T.; Johnston, K. P. *J. Dispersion Sci. Technol.* **2002**, *23*, 65–80.
(22) Psathas, P. A.; Sander, E. A.; Ryoo, W.; Mitchell, D.; Lagow, R. J.; Lim, K. T.; Johnston, K. P. *J. Dispersion Sci. Technol.* **2002**, *23*, 81–92.
(23) Johnston, K. P.; Harrison, K.; O'Neill, M.; Yates, M. Book of Abstracts, 211th ACS National Meeting, New Orleans, LA, March 24−28, **1996** (I&EC-093).
(24) Nave, S.; Eastoe, J.; Penfold, J. *Langmuir* **2000**, *16*, 8733–8740.
(25) McClain, J. B.; Betts, D. E.; Canelas, D. A.; Samulski, E. T.; DeSimone, J. M.; Londono, J. D.; Cochran, H. D.; Wignall, G. D.; Chillura-Martino, D.; Triolo, R. *Science* **1996**, *274*, 2049.
(26) Lee, C. T., Jr.; Ryoo, W.; Smith, P. G., Jr.; Arellano, J.; Mitchell, D. R.; Lagow, R. J.; Webber, S. E.; Johnston, K. P. *J. Am. Chem. Soc.* **2003**, *125*, 3181–3189.
(27) Johnston, K. P.; Cho, D.; da Rocha, S. R. P.; Psathas, P. A.; Ryoo, W.; Webber, S. E.; Eastoe, J.; Dupont, A.; Steytler, D. C. *Langmuir* **2001**, *17*, 7191–7193.
(28) Ryoo, W.; Webber, S. E.; Johnston, K. P. *Ind. Eng. Chem. Res.* **2003**, *42*, 6348–6358.
(29) da Rocha, S. R. P.; Psathas, P. A.; Klein, E.; Johnston, K. P. *J. Colloid Interface Sci.* **2001**, *239*, 241–253.
(30) Bibette, J. *Langmuir* **1992**, *8*, 3178–3182.
(31) Bergeron, V. *J. Phys.: Condens. Matter* **1999**, *11*, R215–R238.
(32) Babak, V. G.; Stebe, M.-J. *J. Dispersion Sci. Technol.* **2002**, *23*, 1–22.
(33) Exerowa, D.; Kruglyakov, P. M. *Foam and Foam Films: Theory, Experiment, Application*; Elsevier: Amsterdam, 1998; Vol. *5*, p 768.
(34) Danov, K. D. *Courses Lect. - Int. Cent. Mech. Sci.* **2004**, *463*, 1–38.
(35) Edwards, D. A.; Brenner, H.; Wasan, D. T. *Interfacial Transport Processes and Rheology*; Butterworth-Heinemann: Boston, 1991.
(36) Bhakta, A.; Ruckenstein, E. *Langmuir* **1995**, *11*, 4642–4652.
(37) Joye, J.-L.; Hirasaki, G. J.; Miller, C. A. *Langmuir* **1994**, *10*, 3174–3179.
(38) Ivanov, I. B.; Kralchevsky, P. A. *Colloids Surf., A* **1997**, *128*, 155–175.
(39) Kabalnov, A.; Wennerstrom, H. *Langmuir* **1996**, *12*, 276–292.
(40) Langevin, D. *Adv. Colloid Interface Sci.* **2000**, *88*, 209–222.
(41) Adkins, S. S.; Chen, X.; Sanders, A.; Nguyen, Q. P.; Johnston, K. P. *J. Coll. Interface Sci.* **2010**, accepted.

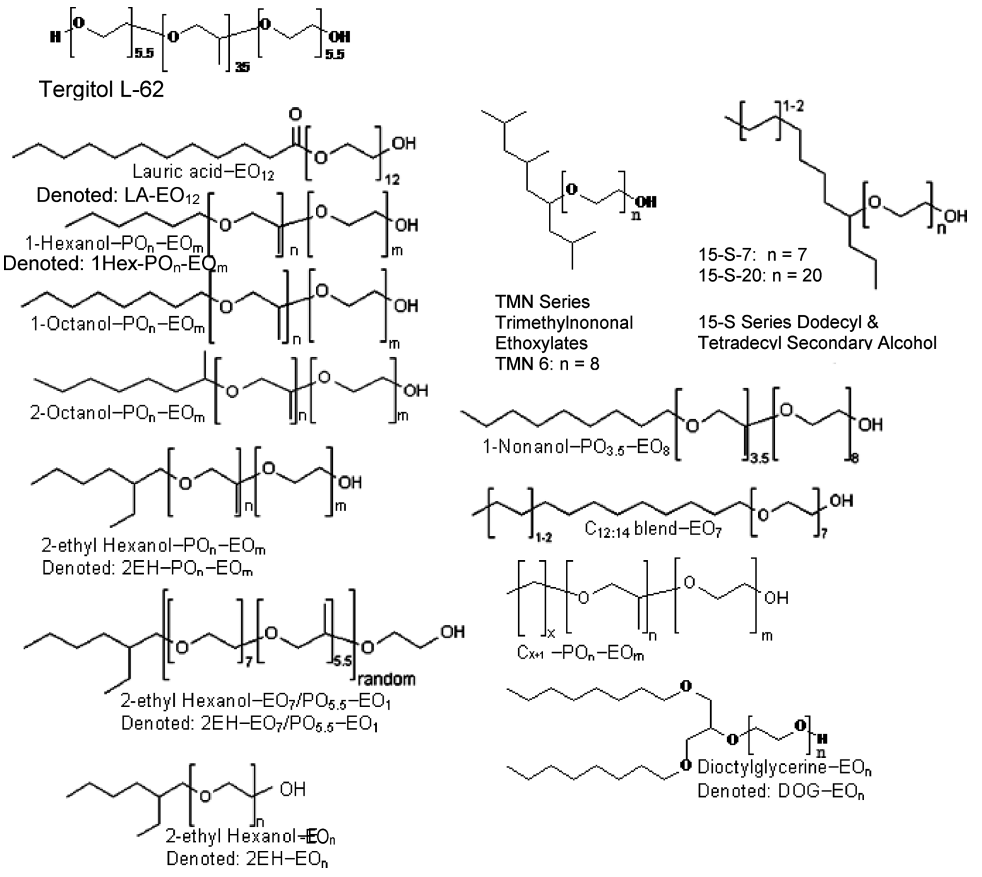

Figure 1. Surfactant structures and naming schemes.

cloud-point temperature was ±1 °C. The cloud-point temperature in brine included 2% NaCl, 0.5% $CaCl_2$, and 0.1% $MgCl_2$ w/w in water.

Interfacial Tension Measurement. The interfacial tension between CO_2 and aqueous surfactant solutions is determined from the axisymmetric drop shape analysis of a captive bubble[42] as previously reported.[41]The surface pressure (π) is the difference between γ_o (no surfactant) and γ (with surfactant). The efficiency of a surfactant (pC20) is calculated as the −log of the surfactant concentration (in units of M) to produce a π of 20 mN/m as determined from the −log(concentration)−π plots. The error in pC20 is ±0.2.

Partitioning of Surfactant into CO_2. A sample of the CO_2 upper phase is taken from a C−W−surfactant system, and the concentration of surfactant in the sample solution was determined by a pendant-drop surface tension measurement below the cmc on the basis of a calibration made for known surfactant concentrations.

C/W Foam Formation and Apparent Viscosity. The partial miscibility between water and CO_2 (without surfactant) is low. At 40 °C, the mole fraction of CO_2 in water is 0.0162 at 50 bar (750 psia) and increases to 0.0243 at 200 bar (3000 psia).[43] The solubility of water in CO_2 is well below 0.01 at all pressures in this study for temperatures up to 50 °C. Therefore, the partial miscibility between water and CO_2 plays a limited role in the formation of C/W foam (also known as C/W emulsions).

The apparatus used to measure foam viscosity is depicted in Figure 2. An Isco syringe pump (model 260D) with a series D pump controller and an HPLC dual-head pump (LDC/Milton Roy consta Metric III) were used to inject the CO_2 and aqueous surfactant solution, respectively, at set flow rates. The mixture of CO_2 and surfactant solution entered a sand pack with hydrophilic pores for foam generation. The sand pack was either a 10.2 cm long, 0.386 cm inner diameter tube packed with prewashed 20−40 mesh nonspherical sand (420−840 μm in diameter) that gives 50 μm pores or a 12.1 cm long, 0.76 cm inner diameter tube packed with nonspherical sand of 125 μm diameter that gives 10 μm pores. For studies of the short-time (1 to 2 min) stability of highly sheared foams (total foam flow rates of 12−15 mL/min reported in Table 2), a sand pack with 10 μm pores was used in which the length was extended to 14.7 cm. The Supporting Information includes information on foam generation in porous media and the equations for estimating pore size in sand packs. Sand was held in place by wire screens affixed to tubing ends. The sand pack for the TMN 6 experiments used packed cotton at the tubing ends instead of the wire screens. Sand packs were rinsed with a few hundred milliliters of ethanol and several liters of DI water until the effluent was surfactant-free. Then surfactant preadsorption was accomplished by running a sufficient volume of surfactant solution (20−50 mL) through the sand pack. In certain experiments, a differential pressure meter was used to measure the pressure drop across the sand pack using a 100 psia diaphragm.

The foam generated in the sand pack flowed through a six-port valve (Valco Instruments, model C6W) followed by a capillary (0.0762 cm inner diameter, 195 cm long). Either a high-range or a low-range differential pressure meter (Validyne model CD23) was used to measure the differential pressure (ΔP) across the capillary. The high-range pressure meter contained either a 100 or 250 psia diaphragm, and the low-range pressure meter contained either a 20 or 50 psia diaphragm. An average ΔP was obtained by averaging the values recorded over at least 2 min while the foam was flowing at approximately steady state, with ΔP varying by less than 15% of the mean value.

The effluent of the capillary flowed through a second six-port valve (Valco Instruments, model C6W) into a stainless steel

(42) Prokop, R. M.; Jyoti, A.; Eslamian, M.; Garg, A.; Mihaila, M.; del Rio, O. I.; Susnar, S. S.; Policova, Z.; Neumann, A. W. *Colloids Surf., A* **1998**, *131*, 231–247.
(43) Wiebe, R. *Chem. Rev.* **1941**, *29*, 475–481.

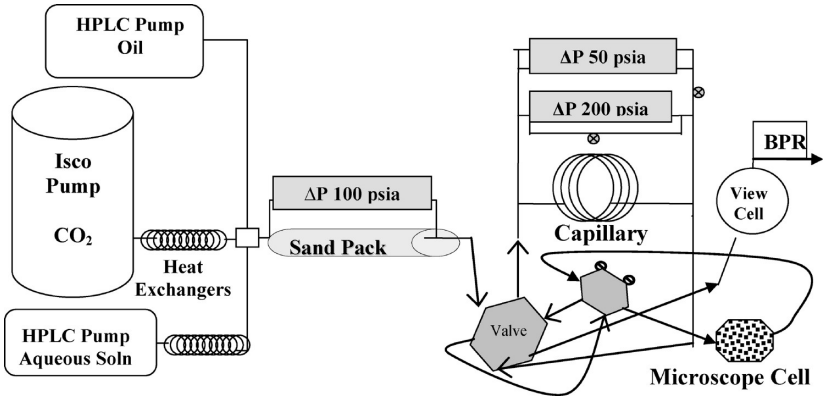

Figure 2. Schematic of the equipment used for foam viscosity and bubble size measurements. BPR stands for the back pressure regulator. The sand pack is used as the foam generator.

cylindrical visual cell with two sapphire windows (0.4 cm path length and 1.8 cm diameter) where macroscopic visual observations of the bulk flowing foam were made. Finally, the foam flowed through the heated (>40 °C with a water bath) back-pressure regulator (BPR) (Swagelok model SS-4R3A adjustable relief valve with either an R3A-E spring for the 2250−3000 psia back pressure setting or an R3A-F spring for 3000−4000 psia), where CO_2 expanded to atmospheric conditions and the surfactant solution was captured for disposal. The system pressure reported was the pressure at the BPR. The BPR was adjusted to set the system pressure. The temperature of the entire apparatus was maintained at ±0.2 °C by use of a water bath equipped with one or more temperature controllers (Julabo, Inc.).

The apparent viscosity of a bulk foam (η_{foam}) is calculated from the known shear rate ($\dot{\gamma}$) and measured pressure difference (ΔP) across the capillary with a length (L) of 195 cm. The shear stress (τ) and shear rate are calculated from $\Delta P R_{cap}/L$ and the velocity gradient (U/R_{cap}), respectively. The average velocity, U, is determined from the total volumetric flow rate of the foam (the sum of the flow rates for the two phases, Q_{total}) divided by the cross-sectional area of the capillary tube. An additional geometric scaling term, $\lambda = {}^1/_8$, is used to calculate the apparent foam viscosity

$$\eta_{foam} = \frac{\tau}{\dot{\gamma}} = \frac{\left(\frac{\Delta P R_{cap}}{L}\right)}{\left(\frac{U}{R_{cap}}\right)}\lambda = \frac{\lambda R_{cap}{}^2 \Delta P}{LU} \qquad (1)$$

where R_{cap} is the capillary tube radius (0.0381 cm).

C/W Foam Microscopy and Stability. The in situ characterization of bubble size and size distribution of the C/W foam was measured by diverting foam flow exiting the sand pack or capillary tube to a high-pressure microscopy cell[44] with the two six-port injection valves. One valve was used to choose the sampling point for the foam, and the second was used to control flow through the microscopy cell. The microscopy cell was mounted on a microscope (Nikon Eclipse ME600). The sapphire windows (Swiss Jewel Company, W6.36, 0.635 cm diameter and 0.229 cm thickness) were separated with foil spacers, creating a path length of approximately 25 μm.[8]

Upon stopping the flow through the cell, images from the microscope were captured via a Photometrics CoolSNAP CF CCD camera connected to a computer. Foam was flowed through the microscopy cell for several cell volumes prior to image recording to ensure that the photographed foam had not aged significantly. The CCD camera was programmed to take photographs at set time intervals (from <1 s to several hours) to provide stability measurements over time. The temperature of the microscope cell and tubing was controlled with electrical heating tape (thermolyne briskheat flexible electric tape, Barnstead/thermolyne) wrapped around the microscopy cell and tubing and thermostatted using a temperature controller (Omega CN7600, Omega) at the same temperature as the water bath.

The images were analyzed with ImageJ software by setting the scale using microscopy standards, adjusting the threshold value of the image, and using the measure particles function. In most cases, bubble areas with a circularity (4π area/perimeter,[2] which is equal to 1 for a circle) of 0.60 or greater were obtained and the dimensions were converted to spherical radii. It was possible to focus on a single layer of bubbles given the low depth of field. Only the top layer of bubbles was measured for the bubbles in the 25 μm cell. Size distribution parameters and average radii were then calculated using the equations below. The minimum bubble size that could be measured had a diameter of 0.4 μm at 50× magnification, 0.88 μm at 20× magnification, and 1.8 μm at 10× magnification; bubbles smaller than these values could not be detected with the microscope and were not sized.

To determine average bubble sizes for a given shear rate, 6−9 microscope images under each condition were analyzed, corresponding to at least several hundred bubbles and up to 10 000 bubbles. The Sauter mean diameter of a given foam, D_{sm}, and the dimensionless polydispersity, U_{poly}, are calculated as follows

$$D_{sm} = \frac{\sum_i D_i{}^3}{\sum_i D_i{}^2} \qquad (2)$$

$$U_{poly} = \frac{1}{D_{med}} \frac{\sum_i D_i{}^3 |D_{med} - D_i|}{\sum_i D_i{}^3} \qquad (3)$$

where D_i is the diameter of a foam bubble and D_{med} is the median bubble diameter of the foam. Number-average diameters, D_{avg}, can also be calculated from the D_i values.

The stability of the foam is measured by photographing a given foam over known time increments. For the short-time (1 to 2 min) stability of highly sheared foams (total foam flow rate of 12−15 mL/min with a sand pack with a 14.7 cm long, 0.76 cm inner diameter tube packed with nonspherical sand of 125 μm diameter in Table 2), a magnification of 50× was used and only the changes in the bubbles in the top layer were measured (reported in Table 2). Again, only the top layer of bubbles was measured. The high flow rate of the foam was varied to produce nearly all small (<0.4 μm) bubbles. When formed, the foam is trapped in the microscopy cell. Initially, the foam is photographed every 1 s

(44) Psathas, P. A.; da Rocha, S. R. P.; Lee, C. T.; Johnston, K. P.; Lim, K. T.; Webber, S. E. *Ind. Eng. Chem. Res.* **2000**, *39*, 2655–2664.

Table 1. Surfactant Properties, C/W Foam Apparent Viscosities (without salt), Initial D_{sm}[a], and Phase Change[b]

	cloud point (°C)				C/W foam at Q_{total} = 6 mL/min							
					24 °C		40 °C		60 °C		70 °C	
surfactant	water	brine	HLB	phase change (°C)	η_{foam} (cP)	D_{sm} (μm)	η_{foam} (cP)	D_{sm} (μm)	η_{foam} (cP)	D_{sm} (μm)	η_{foam} (cP)	D_{sm} (μm)
L62	(32)	27	8.8		33[e]	33	No foam		No foam			
TMN 6 (5%)[h]	(36)[g]	31[g]	12.9		19	18	5[d]	27	No foam			
15-S-7	(37)	32	12.5		11	51	4	46	No foam			
15-S-20	(>100)		16.5		35	21	24	26	13	34	13	19
Lutensol XP70	58		-		4	90	4	42	2	slugs		
C_{8-14}-$PO_{2.5}$-EO_7[f]	60		12.1		10	65	6	50	No foam			
TM NP-9	(54)		(12.9)		35	20	10	18	No foam			
LA-EO_{12}	56		15.2		4	61			No foam			
1Hex-PO_5-EO_9	49		14.6		8	106	18	55	No foam			
1Hex-PO_5-EO_{11}	64		15.4		12	66	24	29	9	46	no foam	
1Hex-PO_5-EO_{13}	78		16		9	63	23	24	12	35	no foam	
1Hex-PO_5-EO_{15}	>80		16.5		12	80	22	25	14	37	15	52
1-octanol-$PO_{4.5}$-EO_8	58		13.4		9	57	No foam					
1-octanol-$PO_{4.5}$-EO_{12}	59		14.9		2	41	No foam					
1-nonanol-$PO_{3.5}$-EO_8	58		13.2		28	43	19	42	No foam			
C_{13}-$PO_{1.5}$-EO_6	34		10.8		8	52			No foam			
C_{11}-PO_2-EO_7	50	42	12.2		20	53	15	46	No foam			
C_{12-14}-EO_7	52		12.1		No foam							
C_9-PO_4-EO_8	56		13		39	34	25	18	No foam			
2-octanol-PO_9-EO_9	45	36	12.4	40−60 ppt	35	47	22	40	No foam			
2-EH-PO_2-EO_4	<24		11.2		3	63	No foam		No foam			
2-EH-PO_3-EO_3	<24		9.7		No foam							
2-EH-PO_5-EO_8	54	40	13.2		22	39	10	50	No foam			
2-EH-PO_9-EO_9	40	34	12.4	40−60 ppt	36	27	20	47	No foam			
2-EH-PO_{12}-EO_{11}	39	32	12.3	24−40 III	34	20	14	47	No foam			
2-EH-PO_5-EO_9	60	54	13.6	40−60 ppt	31	27	25	28	7	61	no foam	
2-EH-PO_5-EO_{11}	71		14.4		48	13	24	46	13	40	no foam	
2-EH-PO_5-EO_{13}	>80		15.1		34	14	25	18	12	41	no foam	
2-EH-PO_5-EO_{15}	>80		15.6		38	22	35	26	14	35	13	38
2-EH-EO_5	<24		12.8		5	26	0.5[c]	48	No foam			
2-EH-$EO_{11.8}$	>80		16.2		15	39	12	28	11	25	10	35
DOG-EO_{12}	46	38	13.9	40−60 ppt	29	30	19	48	24		no foam	

[a] At Q_{total} = 6 mL/min, 2000 psia, 90% v/v CO_2, and 1% v/v surfactant where the coarse sand pack with 50 μm pores was used. [b] As measured in a variable-volume view cell. Legend: ppt means a separate surfactant-rich phase is present, and III means a middle-phase emulsion is present; the surfactant is water-soluble at lower temperatures than those reported. Parentheses indicate manufacturer data. Brine is composed of 2% NaCl, 1% $CaCl_2$, and 0.5% $MgCl_2$ w/w in water. [c] Indicates 87% v/v CO_2. [d] Indicates 88% v/v CO_2. [e] Indicates Q_{total} = 4 mL/min. [f] Indicates 0.5% v/v surfactant. [g] Indicates 1% v/v TMN 6. [h] Indicates no foam with 1% v/v TMN 6 at 24 °C.

for 2 min starting immediately after the flow is stopped. After collection of the foam photographs, the stack of images is converted using the last images with the largest sizes to determine the threshold values for the stack. A circularity of about 0.3 is used. Bubbles greater than 0.4 μm in diameter are measured from the foam photographs for every 5 s to track size changes over time. Then the polydispersity (eq 3), total volume of the bubbles (from the sum of volumes of all of the measured bubbles over 0.4 μm in diameter, that is, $^{\pi}/_6$ times the sum of D_i^3), and D_{sm} (eq 2) were calculated for each of these times. Thus, the total volume is proportional to the cube of the volume-weighted average diameter. The slope dv/dt was determined from the total measured volume of bubbles larger than 0.4 μm as a function of time (Table 2). For the stability of larger bubble sizes over longer times, a single layer of bubbles on the order of 1 to 100 μm was trapped in the microscopy cell and measured over various times. The images are analyzed using the appropriate microscopy scale and circularity (generally 0.5 to 0.6) at known times.

Oil-in-Water and Air-in-Water Emulsions and Foams. For oil−water emulsions containing 90% v/v decane and 10% v/v aqueous solution with 1% v/v surfactant, emulsions were formed in a 20 mL vial and sonicated at the maximum pulse for 20 min. Observations were made immediately after sonication.

The A/W foams were formed by blowing compressed air canisters through a 12 gauge needle affixed to the outlet tube into an aqueous surfactant solution. The aqueous surfactant solution filled 10% v/v of the vial volume with 1% v/v surfactant in DI water. The resulting foam filled the remaining volume of the container.

Results

The measured cloud-point temperatures of the surfactants in water and brine and the calculated HLB (hydrophilic−lipophilic balance) values (using the method of Guo[45]) are presented in Table 1. The measured apparent viscosities (calculated using the measured ΔP in eq 1) of the bulk C/W foams (η_{foam}) in a capillary tube at varying temperatures are also presented in Table 1 with the initial D_{sm} (eq 2) of the foam bubbles. The majority of the foams contained a quality of 90% v/v CO_2, and the foams were stabilized with 1% v/v surfactant (in the aqueous phase) at approximately 2000 psia. The foams were generated with the 50-μm-pore sand pack and at a total foam flow rate (Q_{total}) of 6 mL/min. Most of surfactant structures led to the formation of viscous C/W foams. The formation of the C/W foams is observed to be less challenging than the formation of a W/C concentrated emulsion, where the attractive interactions between the outward-pointing surfactant tails may cause coalescence.[46]

(45) Guo, X.; Rong, Z.; Ying, X. *J. Colloid Interface Sci.* **2006**, *298*, 441–450.
(46) da Rocha, S. R. P.; Psathas, P. A.; Klein, E.; Johnston, K. P. *J. Colloid Interface Sci.* **2001**, *239*, 241–253.

Table 2. Surfactant Properties at the C−W Interface and Stability of Highly Sheared[a] Foams over 120 s[b]c

surfactants	cmc (% w/w)	HLB	γ 0.01% w/w (mN/m)[e]	π 0.01% w/w (mN/m)[e]	A_m (A^2/molecule)[e]	pC2024 °C[e]	pC2040 °C[e]	pC2060 °C[e]	D_{sm}at t_o (μm)	D_{avg} at t_o (μm)	dv/dt, t_f= 120 s (μm^3/s)
2EH-PO_5-EO_9	0.28	13.6	7.5	20.2	219	3.9	4.2	4.5			
2EH-PO_5-EO_{15}	0.28	15.6	5.6	22.1	233	4.3	5.2	5.2	1.3	1.0	140
1Hex-PO_5-EO_{15}	1.47	16.5	8.5	19.2	339	3.5	4.4	5.5	5.3	1.2	130
DOG-EO_{12}	0.015	13.9	4.1	23.6		5.1	5.7		1.3	1.0	50
LA-EO_{12}	0.21	15.2	7.9	19.8		< 3.8			7.3	2.1	> 530
2EH-$EO_{11.8}$	0.99	16.2	12.8	14.9					2.4	1.2	375[d]
2EH-PO_5-EO_{11}	0.42	14.4	7.6	20.1		< 4.0			3.4	1.0	101

[a] Q_{total} = 12−15 mL/min. [b] Sand pack of a 14.7-cm-long, 0.76-cm-inner-diameter tube with 10 μm pores. [c] The conditions are 2000 psia and 24 °C unless otherwise specified. The cmc of the surfactants as determined from the surface tension at the A−W interface is also included. The foams contain 90% v/v CO_2 and 1% v/v surfactant. γ_o for the C−W interface at 24 °C and 2000 psia is 27.7 mN/m. [d] Indicates t_f = 80 s. [e] Indicates data from ref 41.

The viscosities are presented to indicate that the foams were formed, in contrast with low viscosities for mixtures of CO_2 in the absence of surfactant. The effect of the applied stress on viscosity will be described in detail in a future publication. Briefly, we observed shear thinning when the bubble size distribution did not change with shear rate and shear thickening when the bubble size decreased.

Decane−water (50% v/v decane) systems with 1% v/v 2EH-PO_5-EO_9 or 2EH-PO_5-EO_{15} in the aqueous phase formed O/W emulsions that creamed in about an hour at 24 °C. A droplet from the separating upper phase spread on water, not oil, indicating an O/W emulsion. This type of emulsion is expected for surfactants with HLB values of 14 to 15. The experiments were repeated with 90% v/v decane and 10% water. White emulsions were formed with sonication; however, immediately after sonication was stopped, a water-rich phase formed on the bottom. The interfacial tension of decane and water in the presence of 1% w/w 2EH-PO_5-EO_9 in the water phase measured with a captive decane droplet was 2.5 mN/m. The interfacial tension of 1% w/w 2EH-PO_5-EO_{15} at the decane−water interface was 3 mN/m. Despite the interfacial activity of these surfactants, the emulsions were unstable in contrast with the stable pressurized C/W foams under otherwise similar conditions.

A/W foams with 90% v/v air were formed with 1% v/v 2EH-PO_5-EO_9 or 2EH-PO_5-EO_{15} in the aqueous phase. The resulting bubbles were visible with the naked eye and were in the millimeter size range. However, the bubbles at the top of the vial start coalescing immediately after formation, and over half of the foam volume disappears in less than 1.5 min.

Cloud-Point Temperature. The temperatures above which the C/W foam could no longer be formed are reported as a function of the nonionic surfactant structure in Table 1. This temperature is no more than 4 °C above the cloud point for all of the surfactants except DOG-EO_{12}. Observations of the C/W foams formed with 2EH-PO_5-EO_9 showed rapid stability changes when the temperature approached the cloud point. The foam undergoes a transition from a highly stable noncoalescing foam to only slugs of the two phases with only a 1 to 2 °C increase in temperature (~57 °C). The transition of the surfactant from the water phase to a separate surfactant-rich phase at the cloud point greatly reduces the stability of the foam lamella. Bonfillon-Colin and Langevin attribute the rupture of foam films at the cloud point to bridging of the foam films by droplets of the surfactant-rich phase.[47] Furthermore, the presence of salts typically makes the surfactants less soluble and depresses the cloud point (Table 1).

Foam Stability. Table 2 presents the interfacial properties of several surfactants at the C−W interface, including the interfacial tension (γ) and surface pressure (π) at 0.01% w/w surfactant (in the aqueous phase), the area per molecule at the interface (A_m), and the efficiency (pC20) at 2000 psia and 24 °C as previously reported.[41] pC20 is much larger for DOG-EO_{12} compared to that for the other surfactant structures. Foams consisting of 90% v/v CO_2 and 1% v/v surfactant (based on the aqueous phase) at 24 °C and 2000 psia formed with high shear rates (Q_{total} of 12−15 mL/min) through a sand pack with 10 μm pores were studied for stability to coalescence. The high shear, relative to the coarser sand pack and lower flow rates in the studies of Table 1, greatly reduced the initial polydispersity of the foams. The growth rates of these foams (defined as the change in the total sum of bubble volumes) for bubbles with $D_{bubble} > 0.4$ μm measured in the layer in the focal plane, denoted as dv/dt at 120 s, are presented in Table 2 along with the initial D_{sm} and D_{avg} of the foams. Figure 3 presents the change in the volume of bubbles greater than 0.4 μm as a function of time for these surfactants. dv/dt for 2EH-$EO_{11.8}$ is measured for the first 85 s because few foam bubbles smaller than 0.4 μm in diameter persisted beyond this time. Although π of LA-EO_{12} is about the same as for 2EH-PO_5-EO_{11} and 1Hex-PO_5-EO_{15}, it has the highest dv/dt of all of the surfactants. For LA-EO_{12}, the bubble size increases before the foam even reaches the microscope cell. dv/dt for LA-EO_{12} is estimated by assuming that no large bubbles exist at the sand pack exit and that growth on the initial microscopy photograph occurs during the 23 s residence time of flow from the exit of the sand pack to the microscope cell.

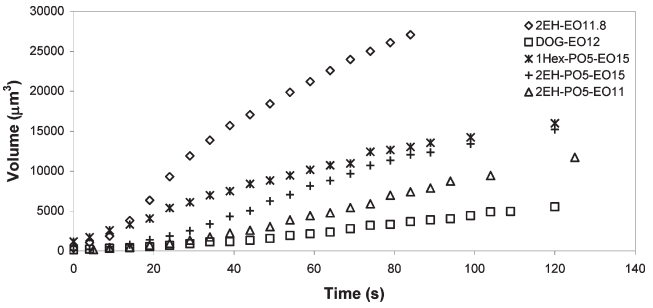

Figure 3. Changes in volume over short times for highly sheared foams stabilized by 2EH-$EO_{11.8}$, DOG-EO_{12}, 2EH-PO_5-EO_{11}, 2EH-PO_5-EO_{15}, and 1Hex-PO_5-EO_{15} with 1% v/v surfactant and 90% v/v CO_2 at 24 °C and 2000 psia. The slopes (dv/dt) are listed in Table 2.

Figure 4 presents the evolution of D_{sm} and U_{poly} over time for the foams stabilized with 1% v/v DOG-EO_{12}, 2EH-$EO_{11.8}$, and 2EH-PO_5-EO_{11}. Figure 5 presents D_{sm}^3 as a function of time for 2EH-PO_5-EO_9 foams of varying surfactant concentration (0.1−1% v/v) at 24 and 55 °C. At 0.1% v/v 2EH-PO_5-EO_9 at 24 °C and 0.2% v/v 2EH-PO_5-EO_9 at 55 °C, no foam was formed; only slugs of the phases were observed. The foam with 0.2% at

(47) Bonfillon-Colin, A.; Langevin, D. *Langmuir* **1997**, *13*, 599–601.

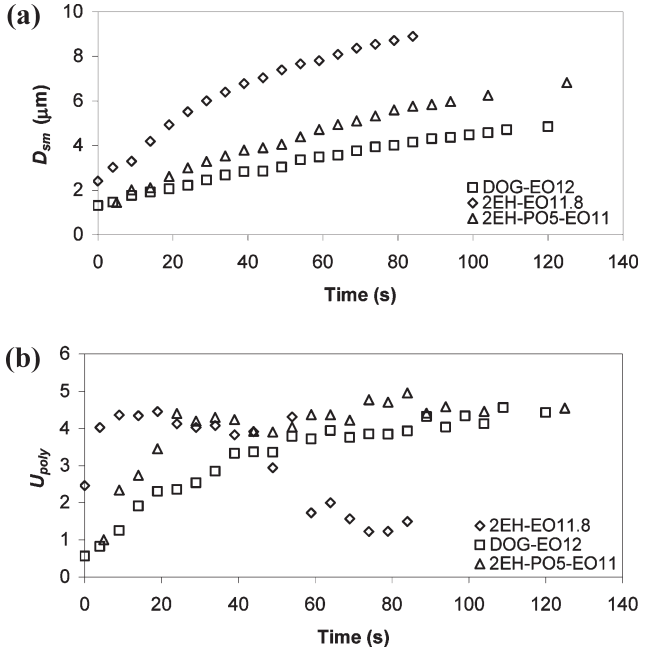

Figure 4. Changes in D_{sm} (a) and U_{poly} (b) over short times of highly sheared foams stabilized by 2EH-$EO_{11.8}$, DOG-EO_{12}, and 2EH-PO_5-EO_{11} with 1% v/v surfactant and 90% v/v CO_2 at 24 °C and 2000 psia.

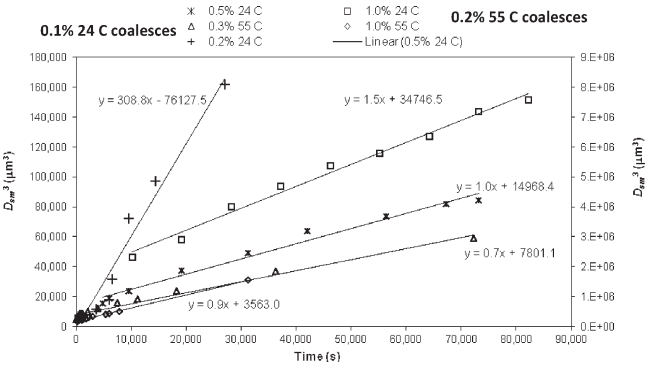

Figure 5. D_{sm}^3 as a function of time for various concentrations (% v/v) of 2EH-PO_5- EO_9 at 24 and 55 °C with 90% v/v CO_2 at 2000 psia where the linear slopes are Ω_3. 0.2% v/v at 24 °C uses right axis. All other conditions use left axis. 0.3% v/v at 55 °C is with brine.

24 °C had larger bubbles and a higher polydispersity relative to the foams with higher concentrations. Micrographs of the DOG-EO_{12}-stabilized foam (Figures 3 and 4) are presented in Figure 6 up to 120 s after the foam is trapped in the microscope. The foams in Figure 7 are stabilized with 2EH-$EO_{11.8}$ where micrographs of up to 91 s after reaching the microscope show more rapid growth. The foam stabilized with LA-EO_{12} is presented in Figure 8 when it initially reached the microscope at 0 s (although the residence time is 23 s from the sand pack).

Table 3 compares the CO_2 distribution coefficients (% w/w surfactant in the CO_2 phase as a fraction of the total surfactant weight in the water−CO_2 system) of 2EH-PO_5-EO_9[48] and 2EH-PO_5-EO_{15} at 2000 psia and 24−75 °C. The initial D_{sm} values of the bulk foams (originally in Table 1) are also given. The measured Ω_3 values (defined as the change in D_{sm}^3 with time, dD_{sm}^3/dt) for

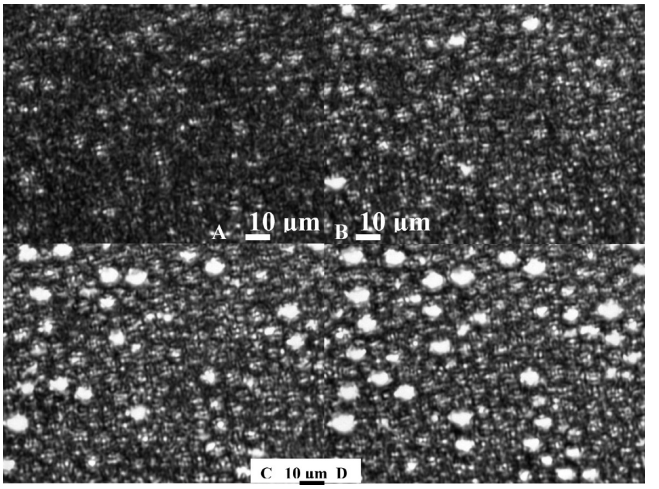

Figure 6. Micrographs of a 90% v/v CO_2 foam stabilized with 1% v/v DOG-EO_{12} highly sheared in a 10 μm pore sand pack at 24 °C and 2000 psia as a function of time at (A) 0, (B) 30, (C) 80, and (D) 120 s. Scale bars are located in the micrographs.

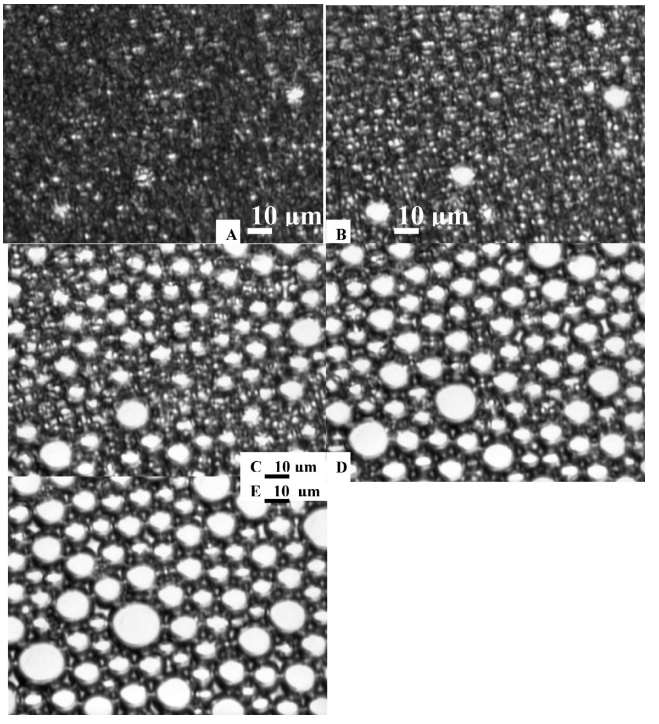

Figure 7. Micrographs of a 90% v/v CO_2 foam stabilized with 1% v/v 2EH-$EO_{11.8}$ highly sheared in a 10 μm pore sand pack at 24 °C and 2000 psia as a function of time at (A) 0, (B) 10, (C) 30, (D) 60, and (E) 91 s. Scale bars are located in the micrographs.

foams with 90% v/v CO_2 and 1% v/v surfactant in the aqueous phase, formed with the 10 μm pore sand pack, were studied through t_f (final time). According to Bancroft's rule,[49] W/C emulsions should be favored because of the high CO_2 distribution coefficients for 2EH-PO_5-EO_9 and 2EH-PO_5-EO_{15} at 24 °C.[32,39] Thus, these C/W foams violate Bancroft's rule. The 2EH-PO_5-EO_9 and 2EH-PO_5-EO_{15} C/W foams were not observed to coalesce in the microscope under any conditions below the cloud-point temperature for the conditions in Table 3.

(48) Chen, X.; Adkins, S. S.; Sanders, A.; Nguyen, Q. P.; Johnston, K. P. Submitted.

(49) Bancroft, W. D. *J. Phys. Chem.* **1913**, *17*, 501–520.

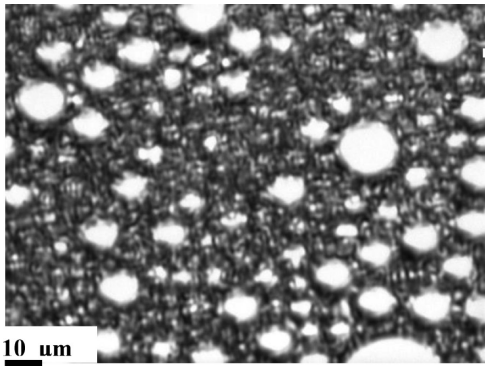

Figure 8. Micrograph of a 90% v/v CO_2 foam stabilized with 1% v/v LA-EO_{12} highly sheared in a 10 μm pore sand pack at 24 °C and 2000 psia at 0 s in the microscope (23 s after formation). The scale bar is located in the micrograph.

Table 3. CO_2 Distribution Coefficient between the Aqueous and CO_2-Rich Phases[a] for 2EH-PO_5-EO_9 and 2EH-PO_5-EO_{15} with Changes in Temperature at 2000 psia and Foam Stabilities in Terms of Experimental Ω_3 Values and U_{poly} Changes Also Included with the Initial and Final Times, t_o and t_f[b]

	T (°C)	CO_2 distribution coefficient (% w/w)	Ω_3 dD_{sm}^3/dt (μm^3/s)	t_f (h)	U_{poly} at t_o	U_{poly} at t_f
2EH-PO_5-EO_9	24	72	1.6	23	2.7	0.3
cloud point	40	30				
61 °C	55		2.5	2.4	1.1	0.6
	60	10				
	75	8				
2-EH-PO_5-EO_{15}	24	58	2.7	8	1	0.4
cloud point	40	11	3.1	27	2.4	2.1
88 °C	60	8				
	70	3	9.9	1	11	0.7

[a] % w/w based on the total surfactant weight. [b] Foams include 1% v/v surfactant and 90% v/v CO_2 at 2000 psia. The foams were formed under the same conditions as in Table 4.

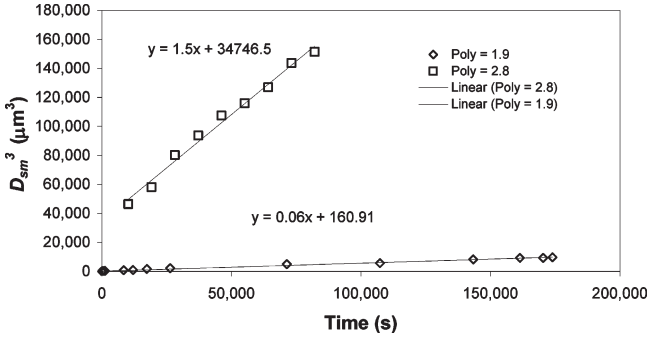

Figure 9. Change in D_{sm}^3 with time for 1% v/v 2EH-PO_5-EO_9 (in the aqueous phase) with 90% v/v CO_2 at 24 °C and 2000 psia at U_{poly} values of 1.9 and 2.8, where Ω_3 values are from the slopes (0.06 and 1.5 μm^3/s, respectively).

Table 4 presents a summary of the stability in terms of Ω_3 for three surfactants at 2000 psia under a variety of conditions, where the foams are stable to coalescence unless otherwise indicated. The behavior shown in Figures 9−11 is also included in Table 4. Figure 9 presents D_{sm}^3 as a function of time for two foams of varying U_{poly} (1.9 and 2.8, respectively) stabilized with 1% v/v 2EH-PO_5-EO_9 and a quality of 90% at 24 °C. Figures 10 and 11 present the changes in D_{sm}, U_{poly}, and D_{sm}^3 as a function of time for over 60 h for foams stabilized with 0.3% v/v 2EH-PO_5-EO_9 (in brine) and 0.3% v/v DOG-EO_{12}, respectively. Lamella rupture was

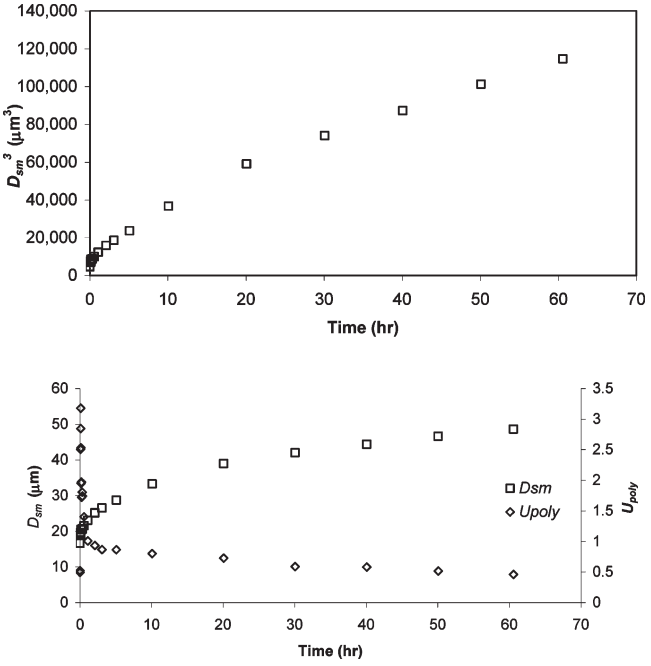

Figure 10. Changes in D_{sm}^3 (top plot), D_{sm} (bottom plot, left axis), and U_{poly} (bottom plot, right axis) with time for a foam stabilized by 0.3% v/v 2EH-PO_5-EO_9 with brine at 55 °C and 2000 psia over 60.5 h.

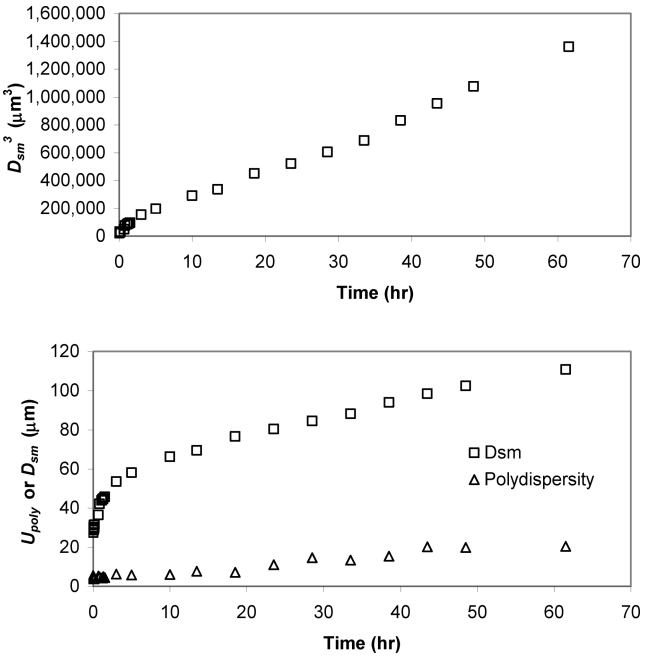

Figure 11. Changes in D_{sm}^3 (top plot), D_{sm} (bottom plot), and U_{poly} (bottom plot) with time for a 0.3% v/v DOG-EO_{12} foam at 24 °C and 2000 psia over 61.5 h.

not observed over the entire time of study for bubbles greater than 0.3 μm in diameter and visible by microscopy. Figure 12 presents the micrographs of the 0.3% v/v DOG-EO_{12} foam over time.

The nonionic surfactants in this investigation have a higher salinity tolerance than ionic surfactants, where salt screens the electrostatic repulsion between films. Moderate levels of salt and divalent ions are often present in reservoirs of interest in CO_2 sequestration and EOR. From Table 4, the 0.3% v/v 2EH-PO_5-EO_9 foam showed insignificant changes in Ω_3 at 55 °C with the

Table 4. Experimental Ω_3 and U_{poly} Values under Various Conditions for 2EH-PO_5-EO_9, 2EH-PO_5-EO_{15}, and DOG-EO_{12} at 2000 psia[a]

							U_{poly}	
surfactants	c (% v/v)	T (°C)	CO_2 (% v/v)	salt (% w/w)	$\Omega_3 d{D_{sm}}^3/dt$ ($\mu m^3/s$)	t_f (h)	at t_o	at t_f
2EH-PO_5-EO_9	0.1	24	90	0	unstable			
	0.2	24	90	0	309	7.5	16.0	4.0
	0.5	24	90	0	2.2	2.7	4.5	0.5
	1	24	90	0	1.6	22.8	2.7	0.3
	1	24	90	0	0.06	48.3	0.6	2.8
	1	24	94	0	49	600 s	1.1	1.1
	0.2	55	90	0	unstable			
	0.3	55	90	0	1.3	1	4.6	1.0
	0.3	55	90	2	0.46	60.5	2.0	0.5
	0.5	55	90	0	0.9	8.7	4.8	0.9
	1	55	90	0	10.5	8.8	7.9	2.4
	1	55	92.4	0	2.5	26	0.8	0.6
	1	55	92.4	2	7.9	1.8	24.5	2.1
2EH-PO_5-EO_{15}	1	24	90	0	2.7	8	1	0.4
	1	24	90	0	4.3	0.5	3.2	1.5
	1	24	90	2	2.9	21.8	2	0.6
	1	24	90	5	2.6	19.5	4.2	0.4
	1	40	90	0	3.1	27	2.4	2.1
	1	70	90	0	9.9	1	2.2	0.4
	1	70	90	2	92	1.8	11.2	0.7
DOG-EO_{12}	0.3	24	90	0	5.8	61.5	6	4.4
	0.2	50	90	0	1.4	6.8	4.8	1
	0.3	55	90	0	2.3	20	7.2	1.1

[a] 0.5% w/w $CaCl_2$ and 0.1% $MgCl_2$ are present unless no salt is added.

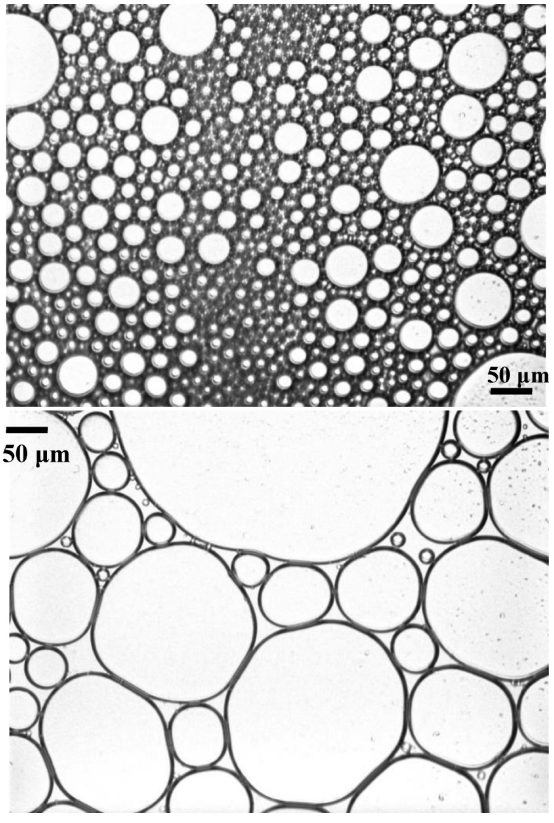

Figure 12. Micrographs of a C/W foam stabilized with 0.3% v/v DOG-EO_{12} at 24 °C and 2000 psia at 0 (top) and 59 h (bottom) after reaching the microscope.

addition of 2% NaCl, 1% $CaCl_2$, and 0.5% $MgCl_2$ w/w (Table 4). Also, the addition of 2−5% NaCl, 1% $CaCl_2$, and 0.5% $MgCl_2$ did not affect Ω_3 values of 2.6−2.9 for 1% v/v 2EH-PO_5-EO_{15} at 24 °C and 2000 psia (Table 4). A drop in the stability of the foam lamella due to salt is observable only at temperatures near the depressed (by salt) cloud point.

Discussion

Surface Pressure and Disjoining Pressure. The adsorption of surfactant at the interface and the reduction in γ must be sufficient to provide stable C/W foams.[8] The surface pressure ($\pi = \gamma_o - \gamma$) is strongly influenced by the degree of surfactant adsorption as described by the surface equation of state (SEOS). For a nonionic surfactant, the SEOS may be expressed as a "hard-disk" reference term (HD) for the headgroup and a perturbation term[50]

$$\pi = \pi_{HD} + (\pi_o + \pi_{el}) \quad (4)$$

where π_o is the solvent−tail interaction term and π_{el} describes electrostatic interactions on the aqueous side of the interface. In the Supporting Information, the solvent−tail interaction is described in terms of the Flory interaction parameter χ. Relative to oils, the weaker solvation of surfactant tails by CO_2, as a result of its low cohesive energy density, leads to larger χ values.[11] An increase in χ will lower π_o and thus π. However, γ will often still be larger for O/W relative to C/W systems as a result of the larger γ_o for the former.

Table 5 presents a summary of the differences between the properties of C/W foams versus A/W and O/W foams or emulsions.[41] The lower γ_o at the C−W relative to both the A−W and O−W interfaces (Table 5) reduces Γ, leading to larger A_m. At the A−W interface, high Γ and strong tail−tail interactions, such as those between linear surfactants, produce high pC20 values. At the C−W interface, where A_m is large, branched and double tails help to occupy volume at the interface to fill in the large gaps

(50) Huh, C. *Eng. J.* **1983**, *23*, 829–847.

Table 5. Comparison of the Properties of C/W Foams with Those of Both A/W and O/W Systems for Branched Hydrocarbon-PO-EO Surfactants

	C/W vs A/W	C/W vs O/W
γ_o	lower	lower
tail solvation	higher	lower
Hamaker constant	higher	higher
π	lower	lower
$\Gamma = 1/A_m$	lower	lower
pC20	similar[a]	similar
P_c	lower	similar
drop size	smaller	similar
drainage:		
capillary suction	lower	lower
gravity	lower	higher (certain ρs)
Marangoni resistance to flow	lower	lower
monolayer bending	N/A	harder
wave formation ("dimples") in film	lower	similar

[a] Data from ref 41.

between surfactant molecules.[51] This volume occupied by the tails helps to separate the two phases to increase π and pC20 (e.g., refer to the case of DOG-EO_{12} in Table 2).[41]

The adsorption of surfactant at the interface influences the disjoining pressure, Π_d, between two CO_2 droplets. The repulsive forces (electrostatic, steric, and structural)[52,34] must counteract the van der Waals attraction between the two film surfaces

$$\Pi_d = -\frac{A_H}{6\pi h_f^3} + 64 \times 10^3 c_{el} N_A kT \tanh^2\left(\frac{e\psi_o}{4kT}\right)\exp(-\kappa h_f) \quad (5)$$

where h_f is the thin film thickness, A_H is the Hamaker constant, c_{el} is the molar concentration of electrolyte, ψ_o is the surface potential of a drop, N_A is Avogadro's number, and κ is the inverse Debye length.[53,54] For aqueous lamella, the EO groups of the surfactant head provide "hard wall" steric repulsion, although the range of this repulsion is short relative to the expected film thickness.[52] As h_f decreases, Π_d increases with increased electrostatic repulsion until a maximum is reached at a critical film thickness (h_{crit}) at the critical disjoining pressure, Π_{crit}. If h_f decreases further, then the van der Waals attraction between the drops can overcome the electrostatic repulsion but only if the steric repulsion is large (with high surfactant adsorption) can the film survive as a Newton black film.[8] For CO_2 bubbles[55] at 24 °C and 2000 psia, the A_H value as determined according to Dhanuka[8] is about 0.04 eV (1 eV = 1.602×10^{-19} J), compared to the 0.003 eV for decane droplets (Table 5).[56,57] Despite this stronger van der Waals attraction, the lamellae were sufficiently thick to provide foam stability.

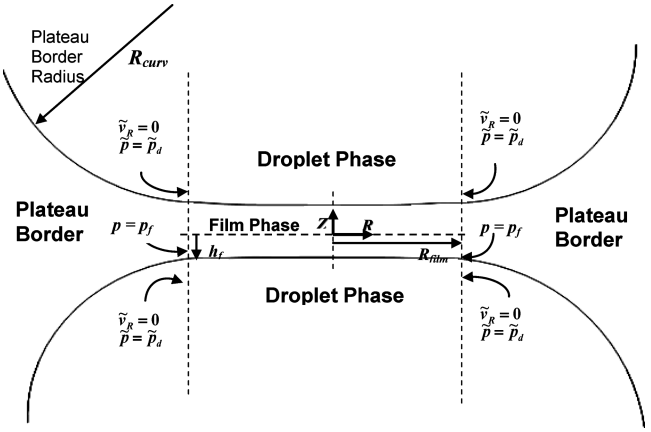

Figure 13. Drawing depicting the symmetric lamellar geometry for thin film drainage between two identical fluid droplets with hydrodynamic boundary conditions.

For nonionic surfactants, the electrostatic repulsion can result from hydroxide ions that naturally adsorb at the A−W and O−W interfaces.[58,59] The C−W interface can also be charged: zeta potentials have been measured for water droplets with nonionic surfactants.[60] The low pH of the C−W system (a value of about 3) will cause significant differences in ion adsorption relative to that at the O−W interface that will require future study to determine the extent to which electrostatic repulsion contributes to lamellar stability.[8]

The disjoining pressure must oppose the Laplace pressure (capillary pressure, P_c) of the foam bubbles. Rapid spinodal decomposition of the films occurs when the Laplace pressure, $2\gamma/R$, exceeds Π_{crit},[30−33] the limiting capillary pressure. For C/W foams, the lower γ will reduce the Laplace pressure relative to Π_d and enhance the stability of the foam relative to A/W and O/W systems for a given drop size. Thus smaller bubbles, in the range of 1−10 μm in Tables 3 and 4, will remain more stable than in the case of A/W foams, where bubbles are typically 0.1 to 10 mm in size and γ is much larger. Aronson et al. found that higher Π_{crit} values lead to stronger foams in porous media with larger flow resistance.[61]

Thin Film Drainage and Marangoni Stabilization. Metastable foams are destabilized by the drainage of the lamellae caused by two effects, gravity and capillary suction into the plateau borders. The much higher density of CO_2 relative to air reduces drainage due to gravity (Table 5). Figure 13 presents a schematic of the lamella between two CO_2 bubbles and the plateau borders with a radius of curvature of R_{curv}.[62] For symmetrical cylindrical film geometry (Figure 13), the difference in pressure between the film and plateau border creates a drainage velocity. Reynolds described a similar drainage velocity for the flow of liquid from between two approaching solid plates

$$V_{RE} = -dh_f/dt = (h_f^3/3\eta_c R_{film}^2)\Delta P_{film} \quad (6)$$

where η_C is the viscosity of the continuous liquid phase, R_{film} is the film radius, and $\Delta P_{film} = 2(P_c - \Pi_d(h))$.[38,40] For a given h_f,

(51) Stone, M. T.; Smith, P. G.; da Rocha, S. R. P.; Rossky, P. J.; Johnston, K. P. *J. Phys. Chem. B* **2004**, *108*, 1962–1966.
(52) Aveyard, R.; Binks, B. P.; Esquena, J.; Fletcher, P. D. I.; Bault, P.; Villa, P. *Langmuir* **2002**, *18*, 3487–3494.
(53) Manoj, P.; Watson, A. D.; Hibberd, D. J.; Fillery-Travis, A. J.; Robins, M. M. *J. Colloid Interface Sci.* **1998**, *207*, 294–302.
(54) Binks, B. P. Emulsions: Recent Advances in Understanding. In *Modern Aspects of Emulsion Science*; Binks, B. P., Ed.; The Royal Society of Chemistry: Cambridge, England, 1998.
(55) Lewis, J. E.; Biswas, R.; Robinson, A. G.; Maroncelli, M. *J. Phys. Chem. B* **2001**, *105*, 3306–3318.
(56) Wohlfarth, C.; Wohlfarth, B. Optical Constants. In *Group III: Condensed Matter*; Lechner, M. D., Ed.; Springer-Verlag: New York, 1996; Vol. *38B*.
(57) *Handbook of Chemistry and Physics*, 90th Edition; Lide, D. R., Ed.; CRC Press: Boca Raton, FL, 2009.
(58) Stubenrauch, C.; von Klitzing, R. *J. Phys.: Condens. Matter* **2003**, *15*, R1197–R1232.
(59) Karraker, K. A.; Radke, C. J. *Adv. Colloid Interface Sci.* **2002**, *96*, 231–264.
(60) Ryoo, W.; Dickson, J. L.; Dhanuka, V. V.; Webber, S. E.; Bonnecaze, R. T.; Johnston, K. P. *Langmuir* **2005**, *21*, 5914–5923.
(61) Aronson, A. S.; Bergeron, V.; Fagan, M. E.; Radke, C. J. *Colloids Surf., A* **1994**, *83*, 109–120.
(62) Sadoc, J. F., Rivier, N., Eds.; *Foams and Emulsions*; Proceedings of the NATO Advanced Study Institute on Foams and Emulsions, Emulsions and Cellular Materials, May 12−24, **1997**, Cargese, Corsica.

the lower γ of the C/W foams produces a smaller P_c and ΔP_{film} and therefore a film drainage V_{RE} relative to both A/W and some O/W systems (e.g., branched C_n-PO_x-EO_y surfactants) as summarized in Table 5. The slower drainage has the potential to enhance the stability of the films against various destabilization mechanisms described below.

Marangoni stabilization (resistance to film drainage) increases with gradients in γ as described by the dilational modulus

$$\varepsilon = -A\, d\pi/dA \quad (7)$$

where A is the interfacial area.[63] For insoluble monolayers or cases where surfactant diffusion and adsorption are slow, the frequency goes to ∞[38] and ε becomes the limiting surface elasticity, $\varepsilon_o = \Gamma\, d\pi/d\Gamma$. For Langmuir adsorption in dilute surfactant solutions,

$$\varepsilon_o = RT(\Gamma_\infty c/c_{0.5}) \quad (8)$$

where Γ_∞ is the saturated adsorption, R is the gas constant, c is the surfactant concentration, and $c_{0.5}$ is the half-saturation value.[63] It was reported that ε is nearly equivalent to ε_o for values of π up to approximately 16 mN/m for $C_{12}E_6$[63] In this dilute regime, ε and ε_o increase with π in a relatively linear fashion and the effect of surfactant diffusion is small. As π increases beyond ~16 mN/m, ε decreases with increasing c and π despite an increase in ε_o. This second regime may be ascribed to surfactant diffusion and adsorption at the film interfaces.[62]

If the timescale for surfactant diffusion and adsorption is shorter than the hydrodynamic timescale that creates the γ gradients, then the Marangoni resistance to the drainage of the foam will be lowered.[64] This scenario arises when the surfactant is very soluble in the dispersed phase, where the diffusion length to the lamellae is small. The rate of film drainage may increase by 10 to 100 to several orders of magnitude when the surfactant is soluble in the dispersed phase relative to when it is soluble in the continuous phase, depending upon the surfactant concentration.[38,40] In addition, Varadaraj et al. demonstrated that the branching of the ethoxylate surfactant tail increased the drainage rate of A/W foams.[65] Emulsions and foams with high drainage rates require sufficiently slow diffusion and adsorption of surfactant at the interface in order for Marangoni flow to oppose the drainage. The slower drainage of the C/W foams appears to make Marangoni stabilization less important than for A/W or some O/W foams or emulsions (Table 5). This factor may have contributed to the high stability of the C/W foams in Table 3 even when the surfactant favored the CO_2 phase, where Bancroft's rule was no longer obeyed.

Branched surfactants with values of π greater than 20 mN/m and large values of pC20 shown in Table 2 stabilize foam more effectively than the less efficient surfactants. A larger π is likely to increase ε_o.[63] A higher ε_o offers the possibility of a higher ε because $\varepsilon_o > \varepsilon$. Thus, an increase in π with surfactant branching has the potential to increase ε, which can be beneficial to increasing Marangoni stabilization. However, it would be necessary to measure ε in order to understand the role of diffusion and how it lowers ε relative to ε_o.

Spatial and Surfactant Density Fluctuations Forming Holes. Spatial fluctuations (interfacial waves or dimples) and surfactant density fluctuations, which are coupled, can lead to spinodal decomposition when the Laplace pressure becomes large relative to or exceeds Π_{crit}.[31] These waves can also lead to asymmetric lamella drainage and film rupture.[37] The Gibbs free energy barrier for a spatial fluctuation depends upon γ, the elastic and shear dilational moduli, and the amplitude and wavelength of the wave. An increase in the elastic and shear dilational moduli dampens surface fluctuations and raises film stability. The smaller film sizes for C/W foam relative to A/W foam reduce the disturbance wavelength and thereby raise the barrier against fluctuations.[31,66] In contrast, the lower γ for the C/W foam lowers the barrier. For a fluctuation in surfactant concentration, the probability of exposing a bare surface of size a is proportional to $\exp(-\varepsilon_o a/kT)$.[31] Thus, an increase in ε_o produced by an increase in π with branching (eq 18) may dampen both spatial and surfactant density fluctuations and thus improve foam stability as observed.[37,40] In addition, the lower interfacial tension gradients for the C−W systems will reduce the growth of the fluctuations.[37]

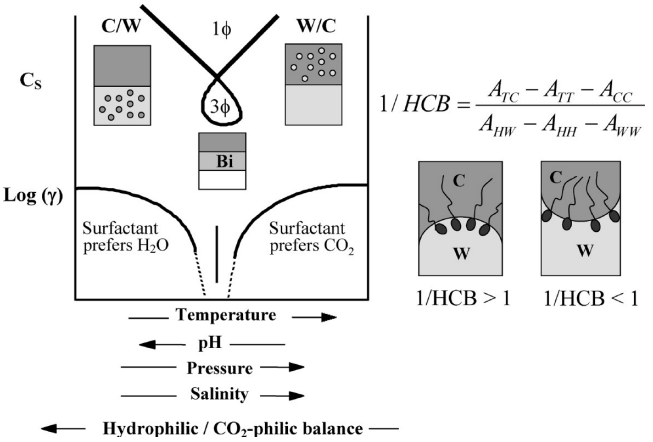

Figure 14. Schematic representation of the effect of formulation variables and HCB (hydrophilic−CO_2-philic balance) on the phase behavior and interfacial tension of a ternary water−CO_2−nonionic surfactant system.

The phase behavior and curvature of a surfactant monolayer and thus the resulting emulsion can be manipulated by varying a formulation variable, such as the hydrophilic−lipophilic balance (HLB) of the surfactant, salinity, and temperature.[67,68] An analogous hydrophilic−CO_2-philic balance (HCB) has been defined and characterized for high-pressure C−W systems.[28,69]

$$1/HCB = \frac{A_{TC} - A_{TT} - A_{CC}}{A_{HW} - A_{HH} - A_{WW}} \quad (9)$$

where A_{ij} is the interaction energy for the various interactions between CO_2 (C), the surfactant tail (T), water (W), and the surfactant head (H). For a CO_2-philic surfactant, where 1/HCB > 1, the surfactant partitions more toward the CO_2 phase and bends about water, forming a W/C emulsion, as shown in Figure 14.[67,70] When 1/HCB < 1, the surfactant prefers the aqueous phase and the interface is concave with respect to CO_2, resulting in

(63) Lucassen-Reynders, E. H.; Cagna, A.; Lucassen, J. *Colloids Surf., A* **2001**, *186*, 63–72.
(64) Saint-Jalmes, A.; Durian, D.; Weitz, D. Foam. In *Kirk-Othmer Encyclopedia of Chemical Technology*; Kroschwitz, J. I., Seidel, A., Eds.; Wiley-Interscience: Hoboken, NJ, 2004; Vol. *12*.
(65) Varadaraj, R.; Bock, J.; Valint, P., Jr.; Zushma, S.; Brons, N. *J. Colloid Interface Sci.* **1990**, *140*, 31–34.
(66) Velev, O. D.; Constantinides, G. N.; Avraam, D. G.; Payatakes, A. C.; Borwankar, R. P. *J. Colloid Interface Sci.* **1995**, *175*, 68–76.
(67) Aveyard, R.; Binks, B. P.; Clark, S.; Fletcher, P. D. I. *J. Chem. Soc., Faraday Trans.* **1990**, *86*, 3111–3115.
(68) Binks, B. P. *Langmuir* **1993**, *9*, 25–28.
(69) Harrison, K. L.; Johnston, K. P.; Sanchez, I. C. *Langmuir* **1996**, *12*, 2637–2644.
(70) Salager, J. L.; Quintero, L. R.; Ennodio; Anderez; Jose, M. *J. Colloid Interface Sci.* **1980**, *77*, 288–289.

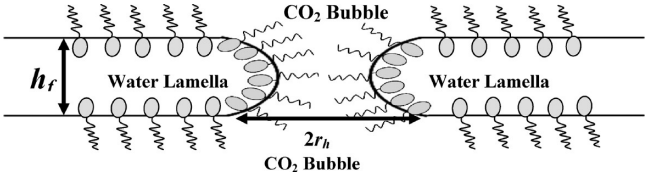

Figure 15. Formation of a hole in a water lamella for a C/W foam. The interactions between the surfactant tails on each side of the hole are a driving force for reducing hole formation.

a C/W emulsion.[8,29,71] The CO_2 density, which may be tuned with pressure and temperature, has a profound effect on the emulsion phase behavior and the curvature of the surfactant monolayer as shown in Figure 14.

For O−W systems and some CO_2 systems, the emulsion undergoes a phase inversion at the balanced state when HLB or HCB = 1, where the surfactant exhibits an equal affinity for both phases[72] and the interfacial tension (γ) is a minimum (Figure 14).[14,21,73−75] The CO_2 distribution coefficients of 2EH-PO_5-EO_9 and 2EH-PO_5-EO_{15} (Table 3) show that these surfactants are very soluble in the dispersed CO_2 phase and the surfactant balance favors CO_2 at lower temperatures (Figure 14). The EO headgroups are moderately soluble in CO_2.[76] Even though these surfactants favored the CO_2 phase, C/W foams were formed and were stable against coalescence for over 60 h (Tables 3 and 4), in violation of Bancroft's rule. da Rocha et al. have also reported the formation of C/W emulsions with CO_2-philic surfactants.[46] They argued that viscous stresses through water were sufficient to shear CO_2 to form bubbles, whereas stresses through CO_2 were too weak to form water droplets.

The coalescence of foam bubbles can occur through a mechanism of hole formation in the lamella. Holes of various radius, r_h, appear and disappear in the thin liquid films because of thermal fluctuations that produce spatial and surfactant density fluctuations.[32,39,77] If the hole radius is $\geq r_h^*$ (the critical radius), then the hole will grow and the foam film will rupture to produce coalescence. The activation energy for the formation of a hole (W_h) includes an energy penalty for the creation of interfacial area and a high interfacial curvature at the edge of the hole (Figure 15). The probability of hole formation is $\exp(-W_h/kT)$.[32,39] Babak et al. added a variable film thickness (h_f) to previous hole-formation theories with the result

$$W^* \cong \frac{h_f^2 \gamma_h^2}{\gamma_p} \qquad (10)$$

where γ_p is the interfacial tension of the planar interface and γ_h is the interfacial tension of a curved border of the hole.[32] The stability of C/W foams is enhanced by the slow drainage of the lamellae that maintains a large h_f (eq 6), which favors a large W^*.

To examine curvature effects, consider a surfactant that favors water over CO_2. In this case for C/W/C films (Figure 15a), there is a large penalty for bending the surfactant about water to open a CO_2 hole. The penalty is much smaller to open up a water hole for a W/C/W film (Figure 15b). Thus, a C/W foam would be favored in accordance with Bancroft's rule as shown by the HCB schematic in Figure 14.

In the balanced state where γ is ultralow ($\ll$0.1 mN/m), O−W emulsions are often very unstable. Here the small amount of energy required to form a hole in the film (eq 10) often leads to rapid coalescence. In the case of C/W emulsions, the energy required to form a hole will be much greater given the much larger γ at the balanced point for a C−W versus O−W interface.[78] Therefore, our C/W emulsions were observed to remain stable even when the surfactant moved through the balanced point with a variation in temperature and pressure (Table 3). Babak et al. cites an interfacial tension of 0.1−1 mN/m as optimal for the stability of 1−10 μm droplets for O−W systems, which is just below the range of the values for our C/W foams.[32]

A novel additional factor is now proposed that contributes to the stability of lamellae in C/W foams. Consider the formation of a hole in the water lamella, as shown in Figure 15. The surfactant tails from the two curved interfaces (hemispheres) are in close proximity to one another. For CO_2, the typical solvation of hydrocarbon tails is not sufficiently strong to prevent the flocculation of spherical water drops in W/C microemulsions and miniemulsions,[27,46,79,80] as explained more fully in the Supporting Information. Thus, flocculation of the tails on the hemispheres in Figure 15 may act to close the hole and prevent coalescence, an important effect not included in eq 10. Alternatively, the penalty for increasing the surface area to form the hole is larger given the limited CO_2 solvation of the surfactant tails. This added stability of water lamella with a CO_2 dispersed phase may likely contribute to the violation of Bancroft's rule, that is, the formation of the C/W foam even when the surfactant prefers the CO_2 phase. This closing of the hole via flocculation is much weaker for O/W emulsions where tail solvation is stronger (Table 5), and the holes can form more readily and cause coalescence, consistent with the unstable emulsions for the 2EH-PO_5-EO_n surfactants. Thus, the phenomena may be somewhat unique to CO_2 as a consequence of weak tail solvation.

Short-Time Stability of C/W Foams. For short-time stabilities, DOG-EO_{12} has the highest π in Table 2 and correspondingly the highest stability (lowest dv/dt value) (Table 2 and Figures 3 and 4). The higher π, which is favored by the double tail, lowers the Laplace pressure, resulting in slower drainage. In addition, a higher π will produce a larger ε_o against fluctuations that produce spinodal decomposition and hole formation. It may also enhance Marangoni stabilization if the higher ε_o provides the potential for a larger ε, although ε is influenced by diffusion.

The dv/dt values of 2EH-PO_5-EO_{11}, 2EH-PO_5-EO_{15}, and 1Hex-PO_5-EO_{15} (with lower π) are slightly higher than that of DOG-EO_{12}; however, the small bubbles persist for over 10−30 min. The polar PO groups in the tails may interact favorable with the CO_2 quadrupoles. For 2EH-$EO_{11.8}$ with the lowest π value, dv/dt is 3 times greater than for 2EH-PO_5-EO_{11}. The small tail of 2EH-$EO_{11.8}$ does not balance the large head of the molecule (indicated by an HLB of 16.1), leading to lower adsorption at the C−W interface.[41] As a result of the lower π, a

(71) Lee, C. T.; Psathas, P. A.; Johnston, K. P.; deGrazia, J.; Randolph, T. W. *Langmuir* **1999**, *15*, 6781–6791.
(72) Psathas, P. A.; Janowiak, M. L.; Garcia-Rubio, L. H.; Johnston, K. P. *Langmuir* **2002**, *18*, 3039–3046.
(73) Aveyard, R.; Binks, B. P.; Clark, S.; Mead, J. *J. Chem. Soc., Faraday Trans. 1* **1986**, *82*, 125–142.
(74) Bourrel, M.; Schechter, R. S. *Microemulsions and Related Systems: Formation, Solvency, and Physical Properties*; Marcel Dekker: New York, 1988; Vol. *30*.
(75) Aveyard, R.; Binks, B. P.; Clark, S.; Fletcher, P. D. I. *J. Chem. Technol. Biotechnol.* **1990**, *48*, 161–171.
(76) O'Neill, M. L.; Cao, Q.; Fang, M.; Johnston, K. P.; Wilkinson, S. P.; Smith, C. D.; Kerschner, J. L.; Jureller, S. H. *Ind. Eng. Chem. Res.* **1998**, *37*, 3067–3079.
(77) Schmitt, V.; Cattelet, C.; Leal-Calderon, F. *Langmuir* **2004**, *20*, 46–52.
(78) Psathas, P. A.; Sander, E. A.; Lee, M. Y.; Lim, K. T.; Johnston, K. P. *J. Dispersion Sci. Technol.* **2002**, *23*, 65–80.
(79) Dickson, J. L.; Ortiz-Estrada, C.; Alvarado, J. F. J.; Hwang, H. S.; Sanchez, I. C.; Luna-Barcenas, G.; Lim, K. T.; Johnston, K. P. *J. Colloid Interface Sci.* **2004**, *272*, 444–456.
(80) Dickson, J. L.; Psathas, P. A.; Salinas, B.; Ortiz-Estrada, C.; Luna-Barcenas, G.; Hwang, H. S.; Lim, K. T.; Johnston, K. P. *Langmuir* **2003**, *19*, 4895–4904.

higher Laplace pressure, and a lower Π_d and ε_o, the coalescence rate is higher (Figure 3 slope).

The stability for LA-EO_{12} relative to that for the more efficient surfactants was lower than expected from the π values alone. π can be used as a guide for surfactant adsorption, which influences the Laplace pressure, ε_o, and the steric and electrostatic repulsive interactions on Π_d; however, additional effects are present. The linear tail of the surfactant is not solvated by CO_2 or bulkier tails.[81] The linear tails block less area of the interface than the EO headgroups, thus the number of EO units and the resulting change in HLB are important. The C_{12-14}-EO_7 surfactant with a linear tail does not form a foam at 1% v/v surfactant and 24 °C (Table 1), whereas the similar methylated C_{8-14}-$PO_{2.5}$-EO_7 stabilizes a foam with only 0.5% v/v surfactant. (Both surfactants have an HLB value of 12.1.) However, when a larger number of EO units are included in the surfactant head, a larger area is occupied at the liquid−liquid interface (given the modest CO_2-philicity of EO groups) and lamella can be stabilized by these higher HLB surfactants. 1% v/v C_{12}-EO_{12} with an HLB of nearly 16 forms a stable, noncoalescing C/W foam (bubble size ranging from 1 to 30 μm) with 90% quality at 24 °C and 2000 psia using a sand pack with 50 μm pores at a total foam flow rate of 6 mL/min.

In most cases, the foam stability decreased markedly at temperatures no more than 4 °C above the cloud point in water, as the surfactant precipitated from water. Only DOG-EO_{12} supports a foam up to about 14 °C above the cloud point (46 °C in Table 1). The large size of the DOG-EO_{12} tail at the C−W interface (due to the dual tail chains that can independently spread at the interface) is more likely to keep the surfactant solvated at the interface as the solubility in water decreases.[41] The polydispersity in the number of EO groups can also decrease the temperature sensitivity.[82] Eventually, as the temperature is raised beyond 60 °C even the surfactants with the higher number of EOs precipitate from water and the foams become unstable.

The foam and emulsion stability decreased with a reduction in surfactant concentration, as is shown in Figure 5 and Table 4. A decrease in c raises ΔP_{film} and lowers Π_d (eq 5), π, and thus ε_o. These factors increase the drainage rates, hole formation, and spinodal decomposition, each of which reduces foam stability. The effect of surfactant diffusion is also lowered, thus ε is closer to ε_o at lower c values. This loss of stability is demonstrated for the 0.1% v/v 2EH-PO_5-EO_9 C/W foam at 24 °C (Figure 5) where slugs of the phases are observed. An increase to 0.2% v/v 2EH-PO_5-EO_9 increases the stability of the foam lamellae, although small bubbles are still relatively unstable. For higher c, much greater stability is present (as seen for the 0.5−1% v/v surfactant in Figure 5). When the interfacial structure of the surfactant changes with the approach to the cloud point (at 55 °C and 2000 psia), the 0.2% v/v 2EH-PO_5-EO_9 foam becomes unstable again with only slugs of the CO_2 and aqueous phases produced. However, coalescence is mitigated with a slight increase in c to 0.3% v/v or higher, even in the presence of salt, which depresses the cloud-point temperature to about 55 °C (Figure 5).

Ostwald Ripening and Long-Term Stability. Foam aging also occurs via Ostwald ripening as a function of the polydispersity in bubble size. Ostwald ripening was described by Lifshitz and Slyozov,[83] followed by Wagner[84] (LSW) for dilute emulsions. The LSW theory assumes that diffusion is from a curved bubble to a flat interface such that

$$\Omega_3 = \frac{dD_{sm}^3}{dt} = \frac{64\gamma D_{diff} S V_m}{9RT} F \quad (11)$$

where D_{diff} is the molecular diffusion coefficient, S is the bulk solubility, and V_m is the molar volume of the dispersed phase (CO_2).[85] A correction factor, F, is included to increase the ripening rate for small diffusion lengths and nondilute conditions.[85] For 90% quality, F is 25.[86] A more rigorous treatment of concentrated polyhedral bubbles, in the case of dry foams, has been presented recently to examine the mean curvature of the films separating the bubbles and the number of bubble faces.[87]

For a given polydispersity, Ω_3 did not vary significantly among the various systems. The relevant properties in eq 11 were similar, with the exception of modest variations in γ. As expected, the variation of the foam polydispersity leads to large changes in the measured Ω_3 for 2EH-PO_5-EO_9 (Figure 9 and Table 4). The slopes (Ω_3) vary nearly 100-fold because of the polydispersity differences between the foams under otherwise similar conditions. Over long times (> 60 h), coalescence was not observed visually for the C/W foams; however, Ostwald ripening was present (Figures 10 and 11). The polydispersity of the foams decreases over time as the small bubbles disappear, which then acts to decrease Ω_3 over ensuing time periods. For example, Ω_3 decreases from 7.5 to 0.5 for the 0.3% v/v 2EH-PO_5-EO_9 foam (Figure 5) as the polydispersity drops from 3.2 to 0.5 over 60.6 h. Here, Ostwald ripening becomes very slow.

Although Ostwald ripening reduces the polydispersity of the foam, coalescence increases the polydispersity (Figure 4, Table 2). The high dv/dt for poor surfactant (low π) 2EH-$EO_{11.8}$ leads to rapid increases in D_{sm} and U_{poly} (Figure 4) as larger bubbles are formed during coalescence. Thus, the driving force for Ostwald ripening increases as well. In Figure 4, U_{poly} increases for 2EH-$EO_{11.8}$ rapidly for the first 10 s and then declines from about 50 s as the Ostwald ripening rate increases. However, U_{poly} of DOG-EO_{12} and 2EH-PO_5-EO_{11} do not experience large drops attributed to Ostwald ripening in this time frame. Here the initial coalescence occurs more slowly, resulting in a lower driving force for Ostwald ripening. At lower concentrations, for example, 0.2% v/v 2EH-PO_5-EO_9 (Figure 5), where some coalescence creates large bubbles and accordingly a higher U_{poly} (4-fold greater than for foams with higher concentrations), a higher Ω_3 (300 $\mu m^3/s$) also results relative to the higher concentrations (Ω_3 values near 1 $\mu m^3/s$). Changes to the foam conditions in terms of temperature and salinity do not vary Ω_3 significantly for a given polydispersity, consistent with small changes in the relevant properties in eq 11.

The results of this study are of practical interest in CO_2 enhanced oil recovery and CO_2 sequestration. For EOR where C/W foams will be in the ground for weeks to months, long-term stability against coalescence is a major goal. Extremely long-term stability is of interest in CO_2 sequestration. Thus, our demonstration of foam stability for several days is an important advance, given that the long-term stability of these foams has rarely been reported. Furthermore, the ability to form stable C/W emulsions selectively when oil is absent and unstable emulsions when oil is present is very beneficial for mobility control. These results may be developed to design surfactants for low CO_2 mobilities in oil-depleted zones and high mobilities in oil-rich zones. Finally,

(81) Dickson, J. L.; Smith, P. G., Jr.; Dhanuka, V. V.; Srinivasan, V.; Stone, M. T.; Rossky, P. J.; Behles, J. A.; Keiper, J. S.; Xu, B.; Johnson, C.; DeSimone, J. M.; Johnston, K. P. *Ind. Eng. Chem. Res.* **2005**, *44*, 1370–1380.
(82) Varadaraj, R.; Bock, J.; Geissler, P.; Zushma, S.; Brons, N.; Colletti, T. *J. Colloid Interface Sci.* **1991**, *147*, 396–402.
(83) Lifshitz, I. M.; Slyozov, V. V. *Sov. Phys. JETP* **1959**, *35*, 331.
(84) Wagner, C. *Z. Elektrochem.* **1961**, *65*, 581–594.
(85) Schmitt, V.; Leal-Calderon, F. *Europhys. Lett.* **2004**, *67*, 662–668.
(86) Marsh, S. P.; Glicksman, M. E. *Acta Mater.* **1996**, *44*, 3761–3771.
(87) Lambert, J.; Cantat, I.; Delannay, R.; Mokso, R.; Cloetens, P.; Glazier, J. A.; Graner, F. *Phys. Rev. Lett.* **2007**, 99.

CO_2-soluble surfactants with distribution coefficients that favor CO_2 can be injected with CO_2 to lower well-bore pressures and minimize surfactant loses to water in the reservoir.

Conclusions

The investigation of morphologies and stabilities (from seconds to days) of C/W foams formed with a variety of nonionic hydrocarbon surfactants by in situ optical microscopy and viscosity measurements, combined with recent measurements of interfacial properties,[41] provides novel insight into foam stability mechanisms. At the C−W interface where a low γ_o creates a lower driving force for adsorption, A_m and thus the contact between phases is greater, relative to the A−W and O−W interfaces. Therefore, reducing the contact between the phases to lower γ by the molecular design of the surfactant is particularly important at the C−W versus A−W and O−W interfaces. Contact may be reduced by increasing the interfacial adsorption of the surfactant or by blocking more interface for a given surfactant adsorption with tail branching or double tails. Branching of the surfactant tail with methyl, propylene oxide, or larger alkyl units reduces the contact of the CO_2 and water phases relative to a linear tail and raises π and similarly the surfactant efficiency (pC20).[41] These changes increase the foam stability, as seen for C_{8-14}-$PO_{2.5}$-EO_7 versus a linear surfactant such as C_{12-14}-EO_7. In addition, EO groups exhibit modest CO_2-philicity and interfacial activity and contribute to reducing the contact between CO_2 and water at the interface, as seen for C_{12}-EO_{11} versus C_{12-14}-EO_7.

Because of the low γ of the C/W foams, micrometer-sized bubbles were formed relative to millimeter-sized bubbles for A/W foams. For surfactants with PO, tail branching, or double-chain tails, for example, 1% v/v DOG-EO_{12}, 2EH-PO_5-EO_9, or 2EH-PO_5-EO_{15}, coalescence of the C/W foam bubbles was rare once the diameter was greater than about 0.5 μm over 60 h. Under similar conditions, A/W foams and decane/water emulsions began coalescing immediately. The greater stability of the C/W foams to coalescence compared with that of the A/W foams may be attributed to the smaller γ and P_c, lower drainage rates, a smaller film size, and a sufficient π and thus limiting elasticity to hinder spatial and surface density fluctuations that lead to coalescence.

In violation of Bancroft's rule, high internal phase C/W foams were stable even when the surfactant preferred the CO_2 phase. This violation may be attributed to three effects. First, the viscous stresses through water can be sufficient to shear CO_2 to form CO_2 bubbles in water, whereas stresses through inviscid CO_2 are often too weak to form water droplets. Second, the low drainage rate for C/W foams, as a consequence of the low γ and thus P_c, makes the loss in Marangoni stabilization from surfactant diffusion from the dispersed CO_2 phase to the aqueous film less important. The last effect is the large resistance to the formation of holes in the aqueous lamellae between the CO_2 domains, as a consequence of strong interactions between surfactant tails on each side of the hole. For surfactants with an HLB relatively close to the balanced state, hole formation in the water lamellae followed by coalescence becomes prevalent for O/W emulsions as γ becomes $\ll$1 mN/m.[39] In CO_2, these ultralow γ values have rarely been achieved, and thus the barrier to create a hole is much larger.

Acknowledgment. This material is based upon work supported in part by the Dow Chemical Co., the STC Program of the National Science Foundation under agreement no. CHE-9876674, the Department of Energy Office of Basic Energy Sciences, the Robert A. Welch Foundation (F 1319), and the Process Science and Technology Center at UT.

Supporting Information Available: Stability of foams with additional micrographs, foam generation, and flocculation. This material is available free of charge via the Internet at http://pubs.acs.org.